MODELING AND PREDICTION OF OCCUPANT KNEE-THIGH-HIP INJURIES

Jialou Hu
Jay Z. Zhao
Amy Klinkenberger
TK Holdings Inc.
United States
Paper Number 09-0334

ABSTRACT

Although extensive modeling efforts have been made in the past decades to predict occupant/pedestrian knee-thigh-hip (KTH) injuries, prediction for the injuries at the tissue level for various loading conditions observed in automotive crashes is still challenging. This study develops model-based tissue injury criteria and a tool to predict occupant KTH injuries subject to different postures and loading rates.

An effective plastic strain based injury criterion with a defined universal threshold was developed for identification of the potential injury locations in the KTH body region. The published cadaver KTH low-rate impact tests at three postures of neutral, adduction, and flexion by UMTRI (University of Michigan Transportation Research Institute) have been simulated with the Takata 50th% male human model. Using the defined criteria, the model predicted the hip-bone and hip-joint fractures for the three postures, were well correlated to those observed from the tests. The KTH impacts were also simulated at two loading rates. The simulation results indicated a possible mode shift of the impact rate-associated injury with assumptions of viscous effects on hip-joint. A high rate impact more likely generates a fracture at the femur shaft; and the impact at a lower rate more likely fractures the hip-joint.

The validated KTH injury criteria and tool were thus applied for accident reconstruction of two vehicle crash cases (full frontal and offset frontal impacts) selected from the NASS/CDS & CIREN database, which caused occupant KTH injuries at AIS 2-3 scale. The simulations match the injury outcomes of the reported field observations.

INTRODUCTION

Lower extremities are the most injured body regions resulting from vehicle crashes. Their long term effect on societal "harm" due to permanent disability and impairment and associated cost is significant. The analysis of NASS-CDS database for the years 1990-1997 by Kuppa et al. [1] indicated that the risk of the AIS 2+ lower extremity injures in all frontal crashes was higher than any other body region. They estimated that the KTH complex injures accounted for ~55% of all the lower extremity injuries annually. Additional analysis of NASS-CDS database for the years 1993-2001 [2] concluded that the complex accounted for 18% of all AIS 2+ injuries sustained by frontal seat occupants involved in frontal automobile crashes and 23% of the associated Life-years Lost to Injury (LLI). Rupp et al. [3-4] estimated from 1995-2000 NASS-CDS database that about 30,000 KTH AIS 2+ injuries occurred annually in frontal crashes, of which approximately 47% were to the hip, and 30% to the thigh. Our latest analysis of NASS-CDS database confirm that lower extremities injuries in the years 2001-2005 remain the highest injured body region, accounting for ~21% of the total injuries and 17% of the AIS 3+ injuries.

Detailed investigations on the real-world automobile crash data indicate that the KTH injury locations and severity vary with crash severity. Although the risk of KTH injuries generally increase with increasing crash severity, quite a large number of the KTH injuries are occurring at crash severities of less than 35 mph [2]. The analysis of the UM CIREN database [5] indicated that the number and percentage of hip injures are particularly high in the 26-35 mph range, while the knee & thigh injuries are more frequent in the lower crash severity of less than 25 mph, which is less than current regulatory and consumer testing levels in FMVSS 208 and NCAP. The KTH injury locations and severity are also affected by other various factors, such as occupant seating posture, age and gender, the KTH contact object type and area, the lower leg/foot loading condition, vehicle crash modes and impact direction, etc. Some of these variables have been investigated in the laboratory PMHS (Post Mortem Human Subject) experiments [6-8].

To develop countermeasures for reduction of the KTH injuries in the real-world crashes, we need to fully understand why and how the KTH injuries occurred, especially in the low severity crashes of delta V less than 25 mph. Such injury mechanisms and outcomes could not be investigated and measured from physical laboratory tests for the anthropomorphic test devices such as Hybrid-III dummies, due to deficiencies in biofidelity of their lower extremities and associated measurable engineering parameter based injury criteria. Therefore, it is very important for us to conduct accident reconstruction for selected vehicle crash cases by computational simulation using a human body model. This requires fully validated human KTH and full body model and associated injury criteria for the tissue failures.

Many occupant/pedestrian KTH or full body models [9-16] have been developed in the past decades. The modeling work was mainly for the tissue material characterization and for the kinematics and response validation. However, few have attempted to develop an injury criterion for estimation of the KTH tissue injuries for various loading conditions observed in automotive crashes. To the our best knowledge none of the previous full body models have been applied to the accident reconstruction of car crash cases with KTH injuries at the tissue level. In previous research, we developed the Takata human body model [9-10] as a tool to evaluate the hard tissue injuries. Although the human model was previously validated at some extent in a series of sled tests simulations, an applicable injury criterion for the KTH tissues was not established, and the models applicability for accident case study and prediction of the occupant KTH injuries in car crashes were not verified.

This research pursued the following objectives:

1. to develop a better human KTH FEA (finite element analysis) model with associated tissue injury criterion applicable for identification of the potential injury locations in the KTH body region and for estimation of the KTH injury modes;
2. using Takata human full body model integrated with newly developed KTH sub-model to conduct accident reconstruction of two vehicle crash cases (full frontal and offset frontal impacts) caused the occupant hip or femur fractures.

KTH MODELING

Figure 1 shows the model of the KTH complex subtracted from the Takata 50th% male human model [9-10]. The hard tissues modeled in the pelvic region included the lumbar, sacrum and coccyx, ilium, ischium, pubis, symphisis pubica, and acetabulum, which have the trabecular bones modeled in solid elements and the cortical bones in shells. The sacroiliac joint was modeled as tied surfaces. The hip joints consisted of the hip joints ligaments (ligament of femur head, the capsular ligaments), the synovial membranes and contact between the femur head and acetabulum. In the thigh and knee regions, the cortical bones of the shaft of the long bones (femur, tibia and fibula) were modeled as solid elements, and those in the head/condyle region were modeled as shells with varying regional thickness. Two joints in each of the knee, the femoro-patellar joint and femoro-tibial joint, were modeled. The femoro-patellar joint consists of the patella, patellar and quadriceps tendons, and the patellar groove. The femoro-tibial joint consists of the femur condyle and articular cartilage, the tibia and fibula and meniscus, as well as the ligaments of ACL, PCL, MCL, LCL. The synovial membranes were modeled as surfaces for soft contact. Various tissue level correlations, such as the pelvis pendulum impact test, femur 3-point bending test, femur head and shaft impact tests, knee pendulum impact test have been implemented previously. The material properties of main tissues were provided [9-10]. In this study, we focus on 1) upgrading the hip joint model for KTH impact in neutral, adducted and flexed postures; and 2) investigating the impact rate effects to the KTH complex through an engineering approach.

1. Simulate the Effects of Hip Posture

The published UMTRI cadaver tests by Rupp, et al [3, 6] were used in upgrading the KTH model. The simulation setup for the impact is shown in Figure 1. The pelvis was held by fixed potting material in the top wing of the pelvis. The knee was impacted at 1.2 m/s and the response of the KTH complex was simulated.

In simulation, the model excluded the knee damage from the impact, as designed in the tests, with the material property management throughout the knee area. The impact loading pattern was measured through the total boundary force of the fixed potting material as well as the contact force of the impactor to the knee. The femur force was measured through the mid shaft of femur. After the KTH complex

model modification and the impactor stiffness management, the 300 N/ms impactor loading profile with the peak force about 6 KN at 40 ms, close to the defined by Rupp [3], was created, as shown in Figure 2.

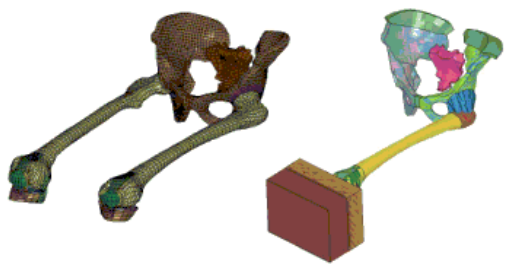

Figure 1. KTH complex and impact model setup.

At first, the responses of the KTH impact in a neutral position were analyzed. Figure 3 illustrates a Von-Mises stress distribution in the cortical bone of acetabulum. The maximum stress above threshold could indicate a potential fracture in the cortical bone. Comparing to the injury observed in the lab test [6], the FEA model reasonably correlates to the test in terms of the fracture location.

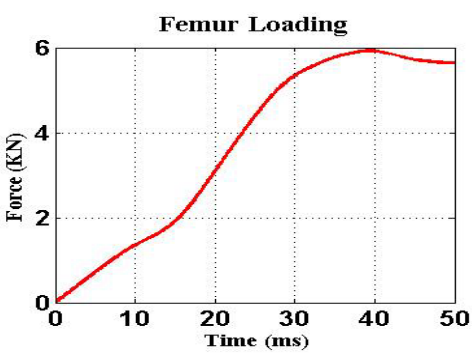

Figure 2. The 300N/ms impactor loading profile simulated.

Then a simulation was conducted of the KTH in three postures: neutral, 10 degree adducted and 30 degree flexed. Figure 4 shows the model top section views and side views of the three KTH postures. Figure 5 gives a typical shear stress distribution at 23 ms for the KTH impact at 30 degree flexed posture. In comparison to the neutral posture (Figure 3), the flexed posture generates a different injury pattern and the FEA indicates the vulnerable area for the flexed posture is at edge of the posterior wall of acetabulum.

Considering that different KTH postures yield different stress distribution patterns and it is difficult to find a unique fracture strength pattern and threshold for the cortical bone fracture of the hip joint, instead an engineering approach was developed to account for the posture variations with FEA feasibility in the strength evaluation, although the approach may reduce the precision in fracture sensitivity and location.

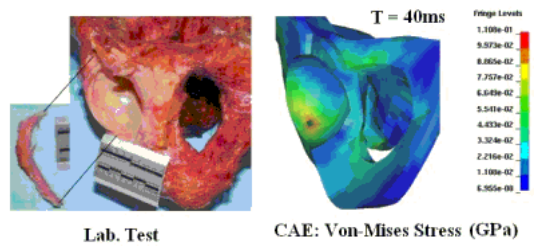

Figure 3. FE-evaluated acetabulum stress distribution vs. lab test injury observation (Lab test courtesy of Rupp).

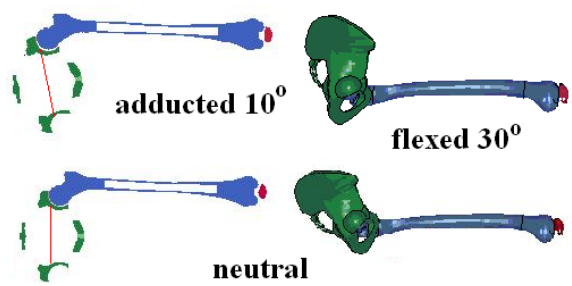

Figure 4. Modeling for the three KTH postures.

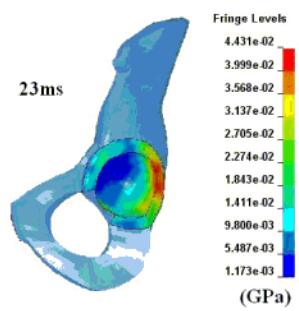

Figure 5. Shear stress yielded at flexed posture around a possible fracture time in acetabulum.

The often-used engineering strength measure in current FEA solvers is plastic strain. A plastic strain of 2.11% was applied to the three postures as a universal strength threshold to the hip fractures for the Takata 50th% KTH model. The forces at the fracture of the acetabulum were calculated, the results are provided as shown in Figure 6. These values match well to the laboratory test results observed by Rupp [3, 6]. Table 1 compares the hip fracture characteristics in the KTH impact to the neutral posture between the FEA and laboratory tests. Table 2 is the summary of the hip tolerance variation

with the other two postures to the neutral posture from the FEA and laboratory tests. In conclusion, the universal criterion of 2.11% plastic strain applied to the Takata 50th% male KTH model provides a reasonable assessment of the hip fracture tolerance for these postures.

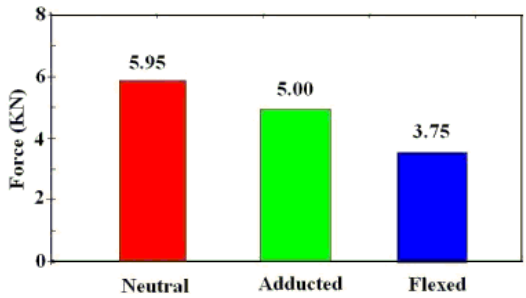

Figure 6. Hip tolerance evaluated with 2.11% plastic strain applied to the Takata 50th% male KTH model.

Table 1.
Hip tolerance from UMTRI test [4] and Takata FEA for KTH impact in neutral posture

Item	Lab. Test [4]		FEA
Test ID	Mean Value	sd	Value
Force at Fracture to all Subjects (KN)	5.70	1.38	
Force at Fracture to Male (KN)	5.96	0.61	5.95
Time to Peak (ms)	38.3	11.5	38
Loading Rate (N/ms)	193	114	198
KTH Stiffness (N/mm)	233	110	328

Table 2.
Hip tolerance percentage change of a given posture to the tolerance of neutral posture: Lab test [5] and FEA

	Neutral	Adducted 10 deg.	Flexed 30 deg.
Lab. Test	0	18 +/- 8%	34 +/- 4%
FEA	0	16%	37%

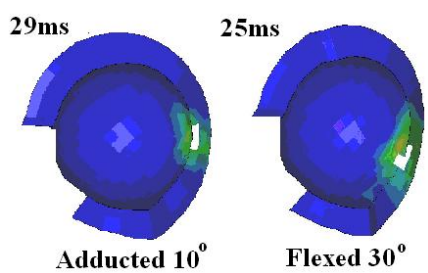

Figure 7. FE-evaluated injury location by element elimination at the time of fracture of acetabulum.

The LS-Dyna element elimination option, a computation method to eliminate those elements whose yielded plastic stains reach the defined threshold in the simulation, enables us to easily identify the injury locations in the KTH impact simulation. Figure 7 shows the fractures of the acetabulum in the KTH impact of the two different postures at the time of each fracture. As expected, the injury occurs at the posterior wall edge of the acetabulum to the adducted and flexed postures.

The above results demonstrate that the Takata 50th% male KTH model is successfully upgraded and applicable for KTH impacts of different postures with a universal strength threshold for injury estimation.

2. Explore Impact Rate Effects to KTH by FEA

As defined in the current Federal Motor Vehicle Safety Standard (FMVSS) 208, the force at mid femur of a midsize-male Hybrid III ATD shall not exceed 10KN in vehicle compliance crash testing. The 10KN force is established from the femur tolerance which is higher than that of the hip joint of the KTH impact studied above. In the KTH frontal impact, the knee contacts the impactor and the force is primarily transferred through the femur shaft to its proximal end. Then, the femoral head transfers the force through articular cartilage to the hip cup. If the acetabular tolerance is reached, the hip joint injures. However, in a significant amount of vehicle accidents with KTH impact, the occupant sustains a femur injury rather than a hip joint injury, one suspected reason is possibly due to the loading rate as mentioned in previous work by Rupp et al. [3].

Along with the Takata KTH modeling efforts, FEA was extended for a preliminary exploration to the impact loading rate effects. The knee damage concern was excluded in this particular study. The impact rate effects could be explored on the mechanical loading performance in the remaining parts of KTH complex: femur, articular cartilage, and hip cup.

Because of its anatomic geometry, the femur could experience a loading eccentricity when impacted resulting in bending. The FEA indicates that approximated uniaxial tensile stress and uniaxial compressive stress can be found along the sides of the shaft as shown in Figure 8. Figure 9 presents the two FEA measurements of the maximum stress. It is known that the bone tensile strength is significantly lower than the compressive strength (1/3 lower). The plot indicates that the vulnerable region of the shaft is at the lateral side with the approximated uniaxial tensile stress.

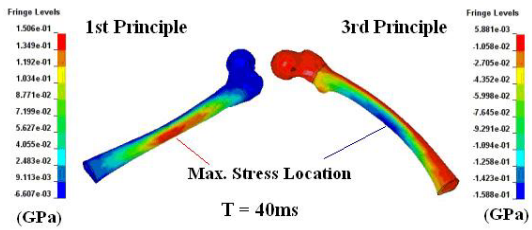

Figure 8. Stress yielded at the shaft during bending.

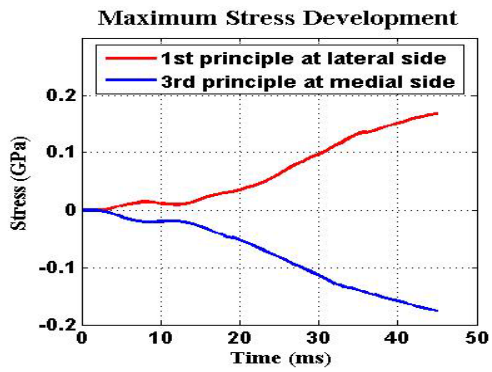

Figure 9. Maximum stress development at the location marked in Figure 8.

In contact with the femur proximal end, the articular cartilage has a biphasic structure, consisting of a solid phase and a fluid phase. Precise modeling of these structures can be challenging in FEA. Instead, a simplified modeling method for their mechanical characteristics was applied. An impact rate related viscous effect could be assumed as a hypothesis for the articular cartilage: the friction coefficient of the contact surface is a function of a relative velocity of the femur head to the acetabulum as shown in Figure 10. A tangential force is distributed at cartilage generated by the impact loading and becomes a part of the boundary conditions to the femur in bending. The boundary condition varies with the relative velocity.

Considered together with the femur bending feature and the assumed mechanical viscous effect of articular cartilage, FEA was conducted to investigate the responses of KTH impact at different rates. Two impact loading patterns, shown in Figure 11, were created in the KTH impact simulations, by varying the impact speed and adjustment of impactor stiffness. The slow rate impact peaked at 6 KN femur loading around 40 ms; and the fast rate impact peaked at 8 KN within 10 ms. The function of Figure 10 for the contact in the hip joint was used in simulations. Material strain-rate properties of the cortical bones of the femur and hip bone were previously implemented in the KTH model.

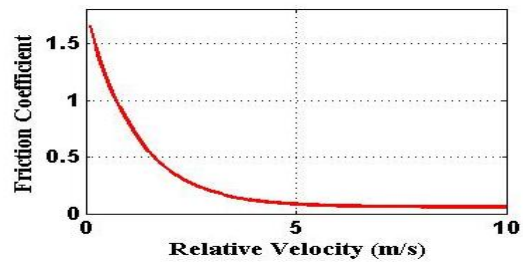

Figure 10. Assumed rate dependent mechanical viscous effect of articular cartilage.

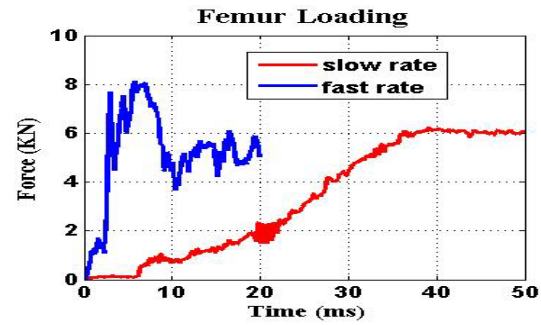

Figure 11. Two impact loading patterns created for impact rate effect study.

Three stress measurements were taken in the analyses: 1) the first principle stress at the maximum stress location on the lateral side femur, 2) the first principle stress at the maximum stress location at acetabulum 3) Von-Mises stress at the maximum stress location in acetabulum. The three locations are indicated in the picture shown in Figure 12.

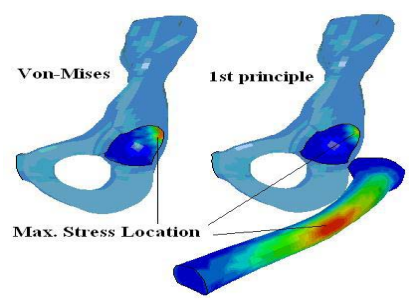

Figure 12. Three stress measurements for strength analysis.

Figure 13 presents the FEA results for the slow rate impact, and Figure 14 presents the data for the fast rate impact. In these plots, the red curve represents the measurement from acetabulum, and the blue represents the measurement from femur. In general, the different patterns of the stress status should not be put together for a direct strength comparison. However, in this particular situation, a fair assumption could be established for the strength

applications by considering that the uniaxial tensile strength to the cortical is the lowest of all.

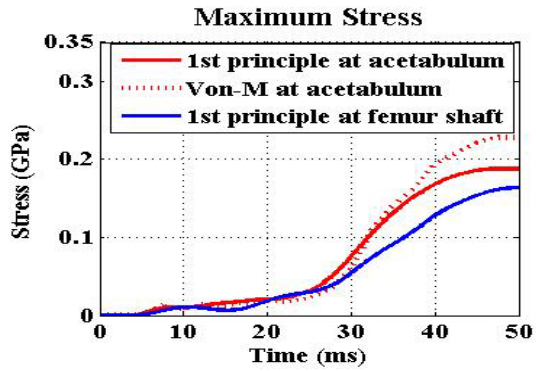

Figure 13. Stress measurements from a slow impact case.

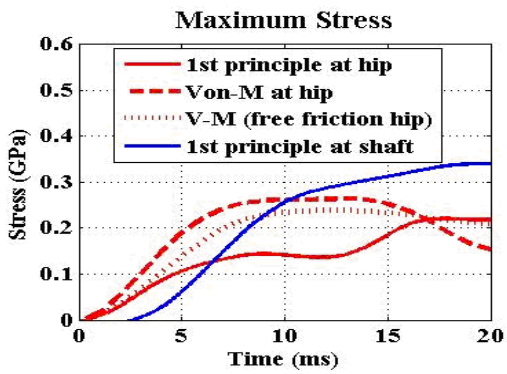

Figure 14. Stress measures from fast rate impact pattern.

For the slow rate impact, Figure 13 shows that the two stress measures of the acetabulum (red curves) are much higher than that of the femur (blue curve). Therefore, the slow rate impact most likely generates a hip joint injury, though the femur may still have a chance to fracture when the tensile stress is close to the acetabulum stresses. For the fast rate impact case in Figure 14, the plot in blue overlaps all the plots in red after 10 ms, which passes the peak time at 7 ms in this case. If the Von-Mises stress of the hip reaches its fracture strength around that time, it is possible to fracture the hip joint. However, tensile stress of the femoral bone with lower strength may also have a chance to fracture at the time. Along with the development of the bending mode, the femur stress continuously moves up; then the chance for the femur fracture would increase significantly. The femur could fracture during the unloading of the impact after the peak force. Figure 14 includes an additional fast rate impact case, presented by dense dot plot in red and marked as "free friction hip". This is a case of free tangential force inside the articular cartilage during the impact. The difference can be found between the two dot plots in red. It indicates the way of the friction influence to the maximum V-M stress level of acetabulum. It seems that the less viscous effect in the tangential plane of hip to a fast rate impact would increase the femur injury chance, because the acetabulum stress level moves down

The universal strength threshold was not tried for the two impact patterns from two kinds of impact rates because it could be strain rate dependence. The factors contributing to the effects of the impact rate in this model are biomaterial strain rate dependence characteristics of cortical bone, the assumption of the relative velocity of hip joint contact, and the strength of the cortical bone associated to the strain rate.

The assumption made for the articular cartilage is based on a physics concern that an easier bending of femur for a fast rate impact is throughout a less tangential restraint in the proximal femur head at the hip joint contact. In other words, an easily sliding of the femur proximal head may let a bending femur more easily reach an unstable condition than those with hardly sliding. Since the assumption needs test data for support, the function as the one in Figure 10 is only considered as an option for the Takata's KTH model.

The FEA offers a preliminary exploration to the KTH impact rate effects through a hypothesis concerned with a mechanical effect modeling of the hip joint. The viscous effect may not be limited to the articular cartilage. Other tissues, like muscle, could also be included.

KTH MODELING APPLICATION CASE 1

With the application of the upgraded Takata Human model from the above efforts, two vehicle accident field cases associated with KTH injury were studied to understand the injury development and injury mechanisms. All the vehicles involved in the cases studies are Honda Accords. A generic FE model of a 1994 Honda is publicly available in the NHTSA website. The model was downloaded and was improved by installing a generic frontal IP (instrument panel) model. The IP model was originally from a 2001 Taurus model available from NHTSA and its knee bolster geometry is modified to represent the Accord for the KTH study. A 1998 Honda Accord 30 mph Flat Frontal Barrier crash was taken from the NHTSA database for the knee bolster model correlation of both driver and passenger sides. The outlines of the vehicle correlation are addressed in Appendix.

Case 1: CIREN Case 830094706

Case 1 concerns an injured driver who was airbag restrained in a single vehicle crash with a relative low delta V impact. A 2003 Honda Accord, 4-door sedan was traveling west on a two-lane, two-way road. The driver of the Honda Accord reportedly fell asleep and crossed the eastbound lane, passed through an intersection and struck a guardrail at the southwest corner of the intersection. Figure 15 depicts the crash diagram of the scene. The impact was classified as a moderate 12 o'clock impact with a 10 degree PDOF (Principle Direction of Force). The WinSmash reconstruction program calculated an equivalent barrier speed of 35 kph (22 mph) which appears to be consistent with the vehicle damage. Figure 16 shows the left and right knee bolster contact.

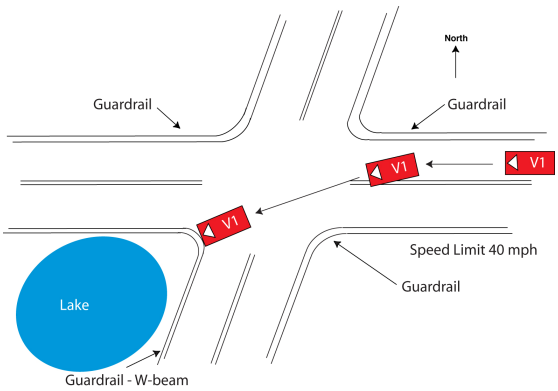

Figure 15. The crash diagram of the 2003 Honda Accord vs. Guardrail.

Figure 16. Left and right knee bolster contact.

Vehicle Crash Re-Construction Simulation

The case occupant: a 57-year-old male, 175 cm (5ft. 9in.), 95 kg (209 lb.), unbelted driver, restrained by the deployed steering-wheel airbag. The driver sustained fractures to the left anterior-lateral 5th and 6th ribs (AIS 2) and an OIS Grade III laceration of the spleen (AIS 3), these injuries are attributed to contact with the steering wheel rim as demonstrated by the rim deformation. The KTH injuries related to this investigation are the right acetabular fracture (AIS 3), right hip dislocation involving the articular cartilage (AIS 2), and right knee meniscus tear (AIS 2). These injuries are attributed to contact with the knee bolster as seen in Figure 16.

A vehicle at velocity 21.74 mph (35 kph) impact 80 degree to a flat barrier was simulated. The flat barrier was modeled with IIHS bumper honeycomb. Figure 18 shows the crash at 140 ms.

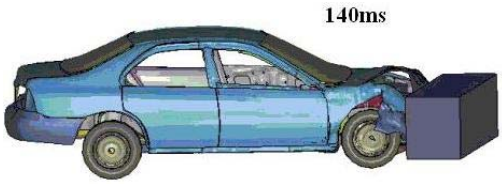

Figure 18. Vehicle impact simulation to a barrier crash in 80 degree at approximately 20 mph.

The vehicle motion profile obtained from the crash simulation is presented in Figure 19, where the positive side direction is from passenger side to driver side. The vehicle starts the impact at nearly 10 m/s speed, and rebounds at about 80 ms while the side velocity reaches highest level about 1m/s.

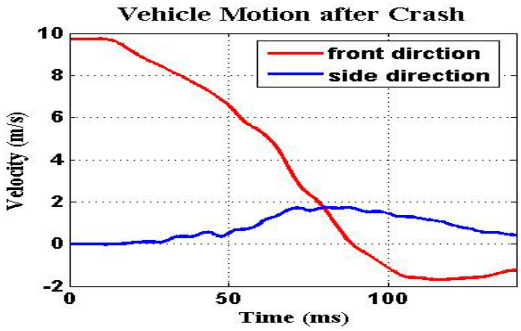

Figure 19. Vehicle velocity profile after crash.

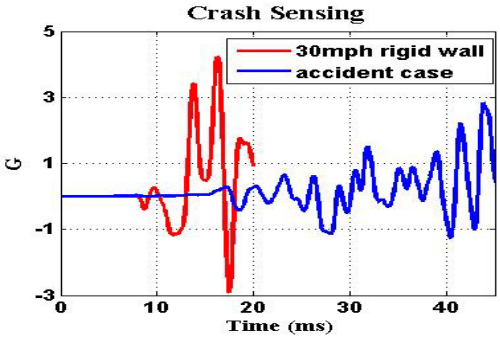

Figure 20. FE-evaluated vehicle frontal crash sensing signal of a rigid wall case and the reconstruction case.

To define the airbag deploying in the accident, crash sensing signals from the center radiator frame were measured through FEA to approach the TTF (time to fire). The signals, resulted from simulations of 30 mph frontal rigid wall impact and the accident case, are presented in Figure 20. The known TTF in the 30mph rigid wall crash is 12 ms. Depended on the algorithm aggressive level, the airbag could be deployed at a time between 26 ms and 38 ms in the crash. In the following addressed simulation, TTF=38ms is used.

During the low severity crash, the compartment entirety was kept without deformation. To simplify the occupant injury simulation in the next step, the vehicle crash can be moved into a simple sled protocol. The motion profile and airbag management were imposed to the sled model with a driver occupant.

Driver Occupant Injury Simulation

Simulation setup for the driver occupant at pre-crash is shown in Figure 21. The driver occupant is not restrained by belt, but by a frontal airbag (Figure 21). The male driver had the similar height but 20 kg more weight than that of the 50th% male human. The Takata 50th% male human model was scaled up without changing the stature in height but to match the total weight of the driver. The driver was assumed at a neutral posture; and initially at the same speed of the vehicle about to crash.

Figure 21. Simulation of unbelted driver in vehicle system.

The simulation showed the occupant moved obliquely forward to the passenger side and toward the windshield during the crash. As a result, the occupant's left side thorax contacts the steering wheel and the head contacts the windshield close to middle; as shown in Figure 22. The kinematics of the occupant is basically consistent with the contacts outlined in the accident case report. The oblique motion of the occupant results in uneven loading to the lower extremities during the crash. Figure 23 shows the FE-evaluated knee contact locations: the right knee impacts into the right corner of knee bolster and the left knee does the other end of the knee bolster of the generic model. Those basically match the contact points of knee bolster shown in Figure 16. Besides, knee meniscus tear (AIS 2) occurred in the right knee of the driver enable to be revealed from FEA for that the right knee was loaded from that contact. On the other hand, the shear stress was not observed in the left knee.

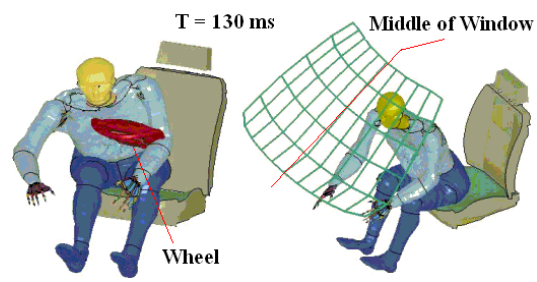

Figure 22. FE-evaluated occupant left thorax bending the wheel and head towards windshield.

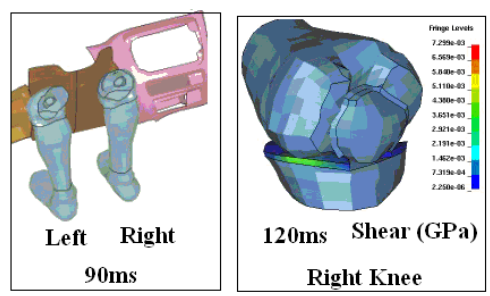

Figure 23. FE-evaluated knee impact location to bolster and right knee meniscus tear from the knee bolster contact.

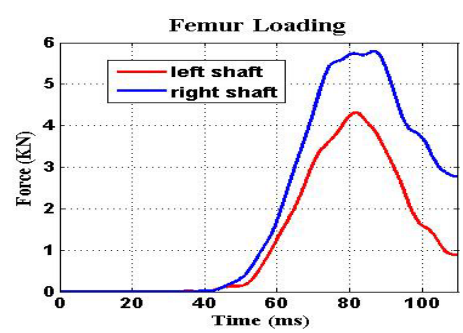

Figure 24. FE-evaluated occupant femur loading.

The femur loads were measured, as shown in Figure 24. Around 80ms, the left femur shaft experiences 5.8 KN and the right shaft experiences 4.2 KN. The loadings start at 40 ms. Therefore, both loading profiles can be categorized as a low rate impact. Figure 25 shows the KTH posture change with time. The occupant has his left KTH in abduction while flexion during the crash. In general, abduction

possesses a relative higher tolerance. The occupant's right KTH is in adduction and flexion with a higher femur loading.

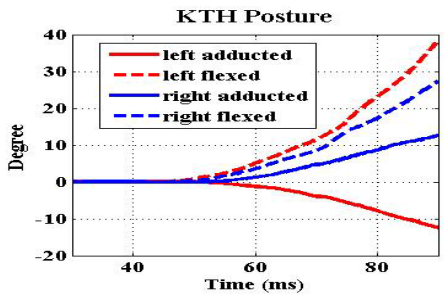

Figure 25. FE-evaluated occupant KTH posture.

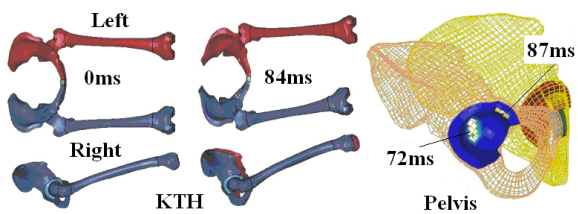

Figure 26. FE-evaluated occupant KTH posture in top and side view; and fracture in right hip joint.

The occupant KTH loading profile and posture status are inclined to a high chance of injury to the right hip joint. The snapshots of animations of the KTH are shown in Figure 26. Fractures were observed in the right acetabulum. The first fracture occurred at 72 ms when the right KTH at posture adducted 8 degree and flexed 10 degree with 5 KN femur loading.

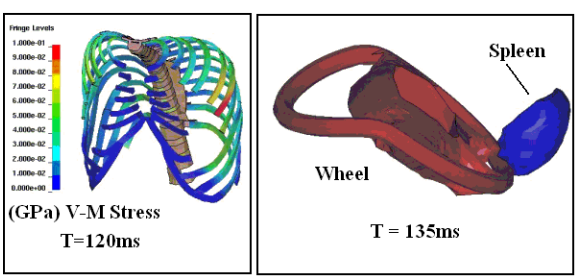

Figure 27. FE-evaluated stress distribution in rib cage, and wheel penetrates into spleen in simulation.

The KTH injury evaluated from the FEA is consistent with the related hip joint injuries reported in the case investigation. In addition to the lower extremity injuries, the FEA reconstructed the left anterior-lateral 5th and 6th ribs (AIS 2) and an OIS Grade III laceration of the spleen (AIS 3) that occurred in the accident due to the wheel rim impact are illustrated by the snapshots in Figure 27.

Overall, the Takata human model with the KTH modeling upgrade successfully predicts the KTH injury for the case application.

KTH MODELING APPLICATION CASE 2

Case 2 concerns an injured frontal passenger without airbag restraint in a two-car crash of a very low delta V impact. The delta V is less than 10 mph. The reported injuries to the front passenger are a left femur fracture (AIS 3) and left lower extremity skin contusion. The remaining two occupants, the driver and a rear-seat occupant, of the same vehicle have no reported injuries.

Case 2: NASS CDS Case 2000-049-268: Honda Accord vs. Honda Accord

A 1991 Honda Accord vs. 1991 Honda Accord: Vehicle 1 was traveling east in the first lane of a two lane undivided driveway, approaching a main cross street. Vehicle 2 was traveling south in the 3rd lane of a 3 lane divided road. Vehicle 1 began to make a left hand turn and contacted the front right corner and right rear side of Vehicle 2. Figure 28 depicts the crash diagram of the scene.

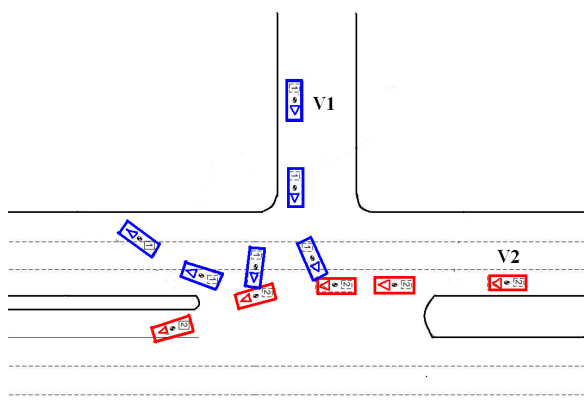

Figure 28. The crash diagram of the 1991 Honda Accord vs. 1991 Honda Accord.

Figure 29. Vehicle 1 damage.

WinSMASH computed a Delta V of 15 kmph/9mph which is consistent with the barrier equivalent speed of 15 kph (9 mph). Vehicle 1 sustained minimal damage as is seen in Figure 29. The case occupant: A 19 year old male 6 ft 0in. (183 cms) 170 lbs (77 kgs) was the right front passenger of Vehicle 1. The occupant sustained a left femur fracture (AIS 3) and left lower extremity skin contusion from apparent contact with the knee bolster.

As Vehicle 1 contacted the right front corner of Vehicle 2, the case occupant moved forward to the left, toward the point of impact. The occupant loaded the lower knee bolster, resulting in a femur shaft fracture. There were no other significant injuries.

Vehicle Crash Re-Construction Simulation

Figure 30 demonstrates the simulation model of a two-car crash in which the injured frontal passenger seated in Vehicle 1. Vehicle 1 impacted at 60 degree and 15 kph. Vehicle 2 moved forward at 45 kph. Vehicle 2 barely contacted the right frontal corner of Vehicle 1.

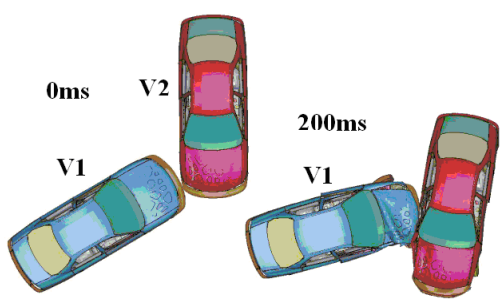

Figure 30. Two-car crash simulation.

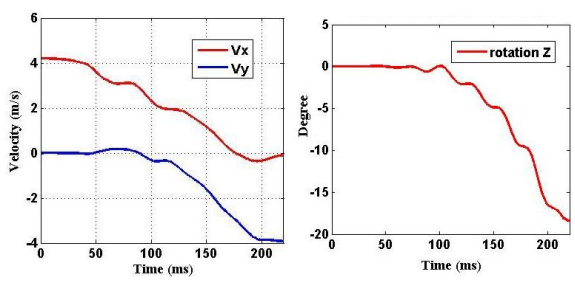

Figure 31. FE-evaluated motion profile including rotation of vehicle 1 post crash.

The motion profiles for Vehicle 1 evaluated from the FEA are presented as shown in Figure 31, where the positive x is from vehicle rear to front, and positive y from vehicle passenger side to driver side. Vehicle 1 at merely 4 m/s hits obliquely to Vehicle 2; and starts moving sideways and spinning toward the passenger side at around 100 ms. It is a very low delta V impact, and the deceleration is only about 4 G.

The occupant injury simulation can be simplified to a simple sled protocol simulation. The calculated motion profiles were imposed to the sled model with a passenger occupant

Passenger Occupant Injury Simulation

The injured frontal male passenger is close to a 50th% male human in weight and size, though he may be a little taller. So the Takata 50th% male human model in a neutral posture was directly applied to the system.

The vehicle was equipped with an automatic shoulder belt and manual lap belt. It is clear that the manual lap belt was not used from the final investigation report. No airbag was available in Vehicle 1. The occupant injury simulations were conducted for a condition of only automatic shoulder belt in use.

The accident happened when Vehicle 1 was making a left hand turn at the intersection. A crash of such low delta V indicates that the driver of Vehicle 1 was trying to stop the vehicle but initiated braking too late to fully stop. Assume the passenger, as a free motion body before the belt is active, possesses an initial velocity which is the same as the vehicle tuning speed before breaking. The passenger could be traveling at up to 30 mph just being about the crash. Therefore, an initial velocity of 12m/s (27mph) is defined for the passenger speed in the following simulation. The belt inertia management feature is triggered at 15ms when the vehicle reached 0.7G of deceleration for the motion profile.

First, the occupant was positioned in a normal seated posture. Under the belt condition for such a low delta V impact, simulation indicated the passenger's movement was restricted to all regions of his body except the knee. The only contact to the IP of the passenger is his knee to the knee bolster. Figure 32 demonstrates the most forward posture that the belted occupant could reach during the crash. The calculated femur loads are also presented and they are about 4KN at 10 to 20ms.

Though this is a fast rate impact, 4KN loading seems unlikely to fracture the femur. However, if the two equivalent loadings mainly act to just one leg, the

total force level then could fracture the shaft. Consider that the frontal passenger could have more flexibility in the posture and position, one candidate posture was defined for the simulation: the passenger abducted each of his thighs in about 5 degrees and turned his whole body 5 degrees toward the outboard side. At this posture, the left knee was closer to the knee bolster than the right knee. The human body model was positioned to replicate the assumed posture from pre-crash simulations. Figure 33 shows the occupant with the new posture in the system. After repeating the simulation, as expected, we have the calculated femur loading by the plots in Figure 34. The left femur experienced about 8KN at a fast rate loading while the right femur load was negligible.

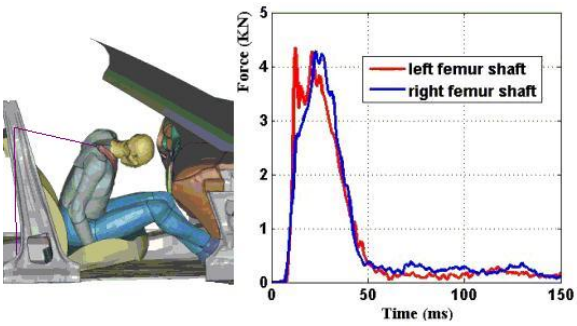

Figure 32. FEA evaluated belted occupant at 140ms and plots of the femur load.

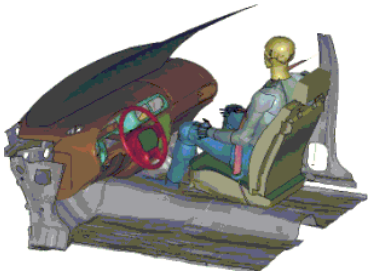

Figure 33. Occupant with one candidate posture leading a possible left femur fracture.

The case was once also evaluated for an unbelted condition as that could be a possible scenario in the field. Through simulation, FEA indicates the unbelted condition is unlikely because being unbelted would have lead to multiple injuries rather than just a single femur fracture.

The potential KTH fracture locations can be referenced to the maximum stress locations shown in Figure 35. The same as the previous strength analysis, the femur takes the first principle stress at the lateral side of the left femoral shaft; and the hip joint takes the Von-Mises stress. Figure 36 presents the time-histories of the stresses. It indicates that the femur has a higher chance of developing a fracture because the femur stress overlaps the acetabulum stress even before the KTH loading peak, and the stress reaches over a potential cortical bone strength tolerance level 125MPa after loading peak time at 22ms.

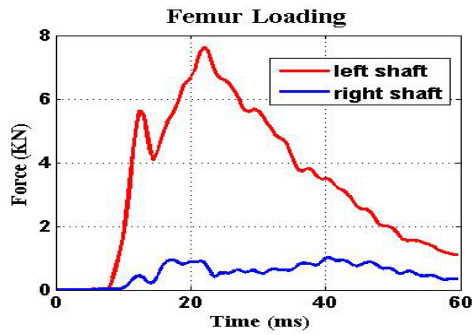

Figure 34. FE-evaluated femur loading profile to a belted occupant at a new posture.

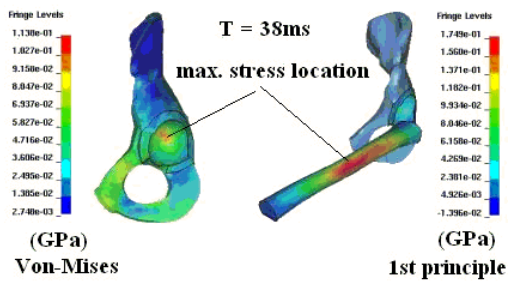

Figure 35. FE-evaluated the stress distribution in left femur and acetabulum at 38ms.

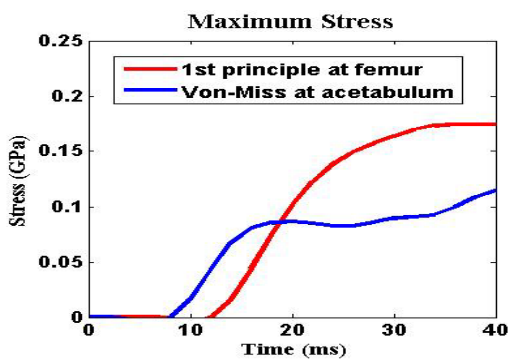

Figure 36. FE-evaluated stress development at the potential fracture locations of femur and acetabulum.

With the application of the Takata 50th% male human model, the field case is successfully investigated. The femur fracture mechanism of the belted occupant in a very low delta V impact is

explored, and the conditions leading to the injury is revealed.

DISCUSSION

Injury protection for KTH impact could be implemented by properly using the available restraint systems. For the first case, if the driver were belted, his kinematics would have managed to reduce the KTH adduction and flexion, and the lap belt would also share a part of knee loading. The driver would have had less chance of experiencing the acetabular fracture. Even if the driver failed to use the belt, if the vehicle was equipped with a knee airbag, it would also improve the KTH impact conditions.

In the knee airbag simulation the research indicates the knee bag is capable to manage the femur loading of less than 3KN for the unbelted heavy occupant. During the knee bag simulation the deploying knee bag did not affect the posture of the right KTH, however, the maximum plastic strain in the acetabulum was 1.548%, less than the threshold value of 2.11%. Therefore, the driver is less likely to have injury at the hip joint with the knee bag application. Figure 37 illustrates the performance.

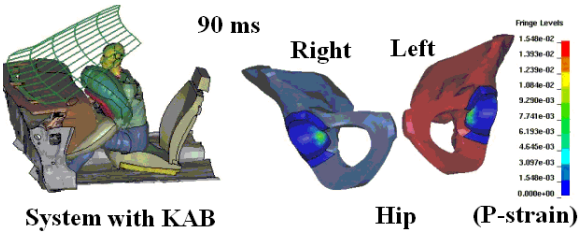

Figure 37. Driver in a system with knee airbag protection and the hip maximum plastic strain status in the protection.

For the second case, if a 3-point belt is equipped with a pretensioner, it would help to control the passengers initial velocity before knee impact and reduce the chance of fracture to the femur.

Though the upgraded Takata KTH model features three key posture of neutral, 10 degree adduction and 30 degree flexion, to be a "full" posture model, correlation to more posture variations may be needed. In the study, a posture computing post-processor tool, generating plots of Figure 25, is used with the universal strength threshold together for the assessment.

FE simulations for case reconstruction may operate with some uncertainties. Since the main target in the study is KTH injury, correlations were more focused on the crash environments directly related to KTH. The KTH injury in both cases occurs early in the crash sequence and later injury experienced in the crash were not concentrated on. To make a complete reconstruction simulation to study all injures in each case a vehicle crash simulation correlation for FMVSS 208 in the study could be further undertaken and some other components in the motion profile would not be ignored.

In this study, we only focused on the hip joint fractures and femur fractures from the PMHS laboratory tests and the real-field case studies. The modeling and model injury prediction capability verification should also be extended to the other body parts of the lower extremities, such as knee, ankle and foot, which are our continued effort for future work on the KTH injury mitigation.

CONCLUSION

The Takata 50th % male human model is upgraded especially for occupant KTH injury prediction or estimation. The model, with the effective plastic strain based injury criterion with a universal cortical bone fracture threshold developed in this study, is capable of predicting effects of occupant postures on the KTH injury patterns and severity under the conditions of UMTRI PMHS KTH impact tests for the neutral, 10 degree adducted, and 30 degree flexed postures.

The model is applied for a preliminary exploration of the effects of impact loading rate on the KTH fracture location and mode, with an assumed mechanical effect modeling for articular cartilage. An engineering approach is established through stress analyses of the femur and hip cup to judge the injury mode due to the rate effects. The engineering approach offers an option for Takata human KTH model applications.

The hip joint fracture and femur fracture are studied by simulating two vehicle crash cases at relative low delta V impacts. The simulations match the injury outcomes of the reported field observations. The occupant injury development and injury mechanisms in these two cases were explored.

ACKNOWLEGEMENT

The authors would like to gratefully acknowledge, to Dr. King Yang at Bioengineering Center of Wayne State University and Dr. Jonathan Rupp at UMTRI for their support for this research. Special thanks to

Gopal Narwani of TK Holdings Inc. for his valuable advice and support.

REFERENCES

[1] Shashi Kuppa, Jing Wang, Mark Haffner, Rolf Eppinger, "Lower Extremity Injuries and Associated Injury Criteria", 17th ESV Conference, Paper# 01-0457, 2001.

[2] Shashi Kuppa, Osvaldo fessahaie, "An Overview of Knee-Thigh-Hip Injuries in Frontal Crashes in The United States", 18th ESV Conference, Paper# 03-0416, 2003.

[3] Jonathan D. Rupp, Reed M.P. et al. "The tolerance of the human hip to dynamic knee loading", Stapp Car Crash Journal, Vol. 46, pp211-228

[4] Jonathan D. Rupp, Carl S. Miller, et al. "Characterization of Knee-Thigh-Hip Response in Frontal Impact Using Biomechanical Testing and Computational Simulations", Stapp Car Crash Journal, Vol. 52, pp. 421-474, 2008.

[5] Mark Sochor, Daniel Faust, Stewart Wang, and Lawrence Schneider, "Knee, Thigh and Hip Injury Patterns for Drivers and Right Front Passengers in Frontal Impacts", Stapp Car Crash Journal, Paper # 2003-01-0164, 2003.

[6] Jonathan D. Rupp, Reed M.P. et al. "Effects of hip posture on the frontal impact tolerance of the human hip joint", Stapp Car Crash journal, Vol. 47, p. 21-33, 2003.

[7] Eric Meyer, Michael Sinnott, etc. "The Effect of Axial Load in the Tibia on the Response of the 90° Flexed Knee to Blunt Impacts with a Deformable Interface", Stapp Car Crash journal, Paper # 2004-22-0003, 2004.

[8] Vijay Jayaraman, Eric Sevensma, etc., "Effects of Anterior-Posterior Constraint on Injury Patterns in the Human Knee During Tibial-Femoral Joint Loading from Axial Forces through the Tibia", Stapp Car Crash journal, Paper # 2001-22-0021, 2001.

[9] Jay Zhijian Zhao and Gopal Norwani, "Development of a Human Body Finite Element Model for Restraint System R&D Applications", 19th ESV Conference, Paper# 05-0399, 2005.

[10] Jay Zhijian Zhao and Gopal Norwani, "Biomechanical Analysis of Hard Tissue Responses and Injuries with Finite Element Full Human Body Model", 19th ESV Conference, Paper# 07-0354, 2007.

[11] Yuji Kikuchi, Yukou Takahashi, etc., "Development of a Finite Element Model for a Pedestrian Pelvis and Lower Limb", SAE Paper #2006-01-0683, 2006.

[12] Philippe Beillas, Paul Begeman, etc., "Lower Limb: Advanced FE Model and New Experimental Data" Stapp Car Crash journal, Paper #2001-22-0022, 2001.

[13] Yuichi Kitagawa, Junji Hasegawa, etc. "A Study of Knee Joint Kinematics and Mechanics using a Human FE Model", Stapp Car Crash journal, Paper #2005-22-0006, 2005.

[14] Costin Untaroiu, Kurosh Darvish, etc., "A Finite Element Model of the Lower Limb for Simulating Pedestrian Impacts", Stapp Car Crash journal, Paper #2005-22-0008, 2005.

[15] Chia-Yuan (Mark) Chang, etc., "Development of a Finite Element Model to Study the Effects of Muscle Forces on Knee-Thigh-Hip Injuries in Frontal Crashes", Stapp Car Crash journal, Paper #2008-22-0022, 2008.

[16] Jesse Ruan, etc., "Impact Response and Biomechanical Analysis of the Knee-Thigh-Hip Complex in Frontal Impacts with a Full Human Body Finite Element Model", Stapp Car Crash journal, Paper #2008-22-0022, 2008.

APPENDIX: VEHICLE IP CORRELATION

NHTSA Vehicle Database #V2836 of 1998 Honda Accord 30 mph into a flat frontal barrier is taken for vehicle system model correlation. The test in NHTSA was to evaluate the vehicle and occupant dynamics during a flat frontal barrier test at 30 mph. The vehicle was instrumented with 13 accelerometers to measure vehicle acceleration. Squib current was also collected to measure fire times of the airbag. The vehicle contained two instrumented Hybrid III 50th% percentile ATD, instrumented with head and chest accelerometers, chest deflection potentiometers, left and right femur load cells and upper neck load cells. The collected vehicle and occupant data was used to verify the vehicle model for simulation.

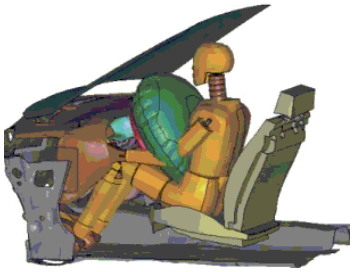

Figure 38. 30 mph flat frontal barrier FE simulation.

FEA was conducted to correlate the test for getting a reasonable mechanical property of knee boaster to use for the accident case simulation. The system model including Hybrid III 50th% dummy, airbag, and generic IP is shown as Figure 38. The dummy chest G is monitored in the simulation to make a basic assessment of correlation of the dummy kinematics to the test. The dummy femur loads are measured for the assessment of the mechanical properties of knee bolster.

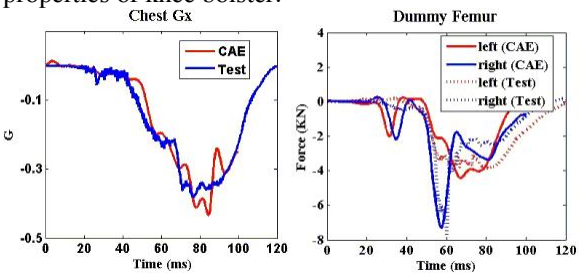

Figure 39. Driver performance correlation for chest G and femur loading of dummy.

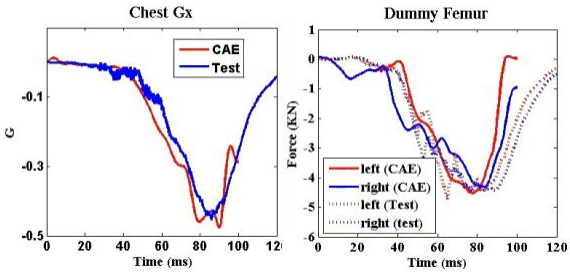

Figure 40. Passenger performance correlation for chest G and femur loading of dummy.

The correlations of the dummy performance to the both driver and passenger sides are obtained reasonably. The results for the driver side are presented in Figure 39, and passenger side at Figure 40. The FE correlations offer a fair base for the accident case simulation.